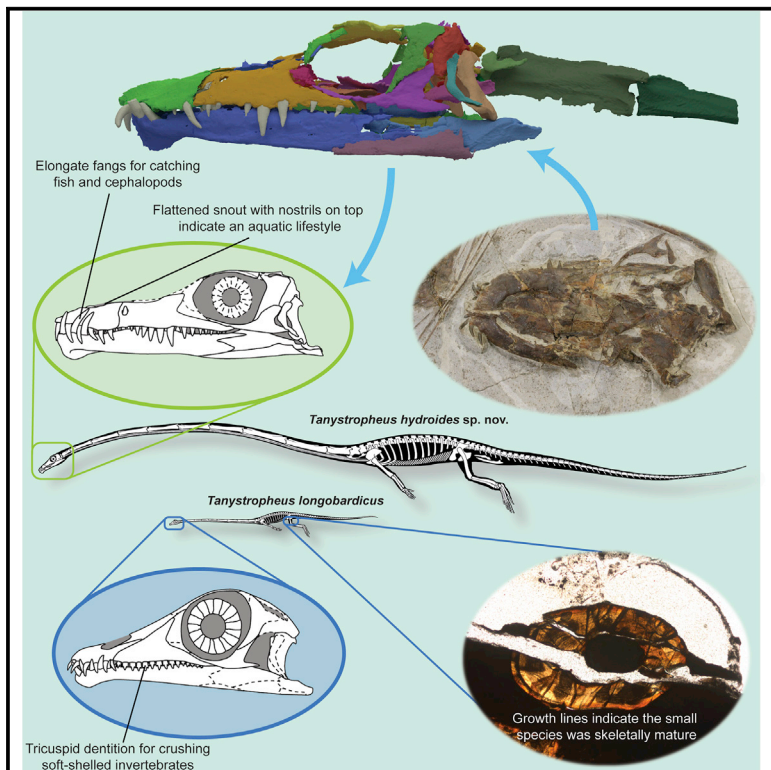


## Aquatic Habits and Niche Partitioning in the Extraordinarily Long-Necked Triassic Reptile *Tanystropheus*

### Graphical Abstract



### Authors

Stephan N.F. Spiekman,  
James M. Neenan, Nicholas C. Fraser,  
Vincent Fernandez, Olivier Rieppel,  
Stefania Nosotti, Torsten M. Scheyer

### Correspondence

stephanspiekman@gmail.com

### In Brief

Spiekman et al. present a new cranial reconstruction of the extremely long-necked Triassic reptile *Tanystropheus*. Its skull shows several adaptations for an aquatic lifestyle. Furthermore, its morphology reveals that small and large specimens of *Tanystropheus* represent separate species with different diets, thus indicating niche partitioning.

### Highlights

- Two species of *Tanystropheus* co-occurred in a Middle Triassic coastal habitat
- The skull of the larger species shows it was an aquatic ambush predator
- Bone histology indicates that the small species was skeletally mature
- The two species fed on different prey, representing a case of niche partitioning

## Report

# Aquatic Habits and Niche Partitioning in the Extraordinarily Long-Necked Triassic Reptile *Tanystropheus*

Stephan N.F. Spiekman,<sup>1,8,\*</sup> James M. Neenan,<sup>2</sup> Nicholas C. Fraser,<sup>3</sup> Vincent Fernandez,<sup>4,5</sup> Olivier Rieppel,<sup>6</sup> Stefania Nosotti,<sup>7</sup> and Torsten M. Scheyer<sup>1</sup>

<sup>1</sup>University of Zurich, Paleontological Institute and Museum, Karl-Schmid-Strasse 4, Zurich 8006, Switzerland

<sup>2</sup>Oxford University Museum of Natural History, Parks Road, Oxford OX1 3PW, UK

<sup>3</sup>National Museums Scotland, Chambers St, Edinburgh EH1 1JF, UK

<sup>4</sup>European Synchrotron Radiation Facility, 71 Avenue des Martyrs, Grenoble 38000, France

<sup>5</sup>The Natural History Museum, Cromwell Road, London SW7 5BD, UK

<sup>6</sup>Field Museum of Natural History, 1400 S Lake Shore Dr, Chicago, IL 60605, USA

<sup>7</sup>Museo Civico di Storia Naturale di Milano, Corso Venezia 55, Milan 20121, Italy

<sup>8</sup>Lead Contact

\*Correspondence: [stephanspiekman@gmail.com](mailto:stephanspiekman@gmail.com)

<https://doi.org/10.1016/j.cub.2020.07.025>

## SUMMARY

*Tanystropheus longobardicus* is one of the most remarkable and iconic Triassic reptiles. Mainly known from the Middle Triassic conservation Lagerstätte of Monte San Giorgio on the Swiss-Italian border, it is characterized by an extraordinarily long and stiffened neck that is almost three times the length of the trunk, despite being composed of only 13 hyper-elongate cervical vertebrae [1–8]. Its paleobiology remains contentious, with both aquatic and terrestrial lifestyles having been proposed [1, 9–12]. Among the *Tanystropheus* specimens, a small morphotype bearing tricuspid teeth and a large morphotype bearing single-cusped teeth can be recognized, historically considered as juveniles and adults of the same species [4]. Using high-resolution synchrotron radiation microtomography (SRμCT), we three-dimensionally reconstruct a virtually complete but disarticulated skull of the large morphotype, including its endocast and inner ear, to reveal its morphology for the first time. The skull is specialized toward hunting in an aquatic environment, indicated by the placement of the nares on the top of the snout and a “fish-trap”-type dentition. The SRμCT data and limb bone paleohistology reveal that the large morphotype represents a separate species (*Tanystropheus hydrooides* sp. nov.). Skeletochronology of the small morphotype specimens indicates that they are skeletally mature despite their small size, thus representing adult individuals of *Tanystropheus longobardicus*. The co-occurrence of these two species of disparate size ranges and dentitions provides strong evidence for niche partitioning, highlighting the surprising versatility of the *Tanystropheus* bauplan and the complexity of Middle Triassic nearshore ecosystems.

## RESULTS

### Systematic Paleontology

Diapsida Osborn, 1903 [13].

Archosauromorpha von Huene, 1946 [14].

Tanystropheidae Camp, 1945 [15].

*Tanystropheus* von Meyer, 1852 [16].

*Tanystropheus hydrooides* sp. nov.

### Etymology

“Hydra” refers to the long-necked mythical sea monster of Greek antiquity; the suffix “-oides” means “related to” or “resembling” in ancient Greek. The name refers to the resemblance of *T. hydrooides* to this famous mythological creature.

### Holotype

PIMUZ T 2790, a semi-articulated specimen consisting of a virtually complete yet strongly compressed skull and the first eight cervical vertebrae.

### Referred Material

PIMUZ T 2787, PIMUZ T 2793, PIMUZ T 2818, PIMUZ T 2819, PIMUZ T 183, SNSB-BSPG 1953 XV 2, MSNM V 3663. A synonymy list is provided in [17] (as the large morphotype of *T. longobardicus*).

### Locality

Monte San Giorgio on the border of Switzerland (canton Ticino) and Italy (Lombardy).

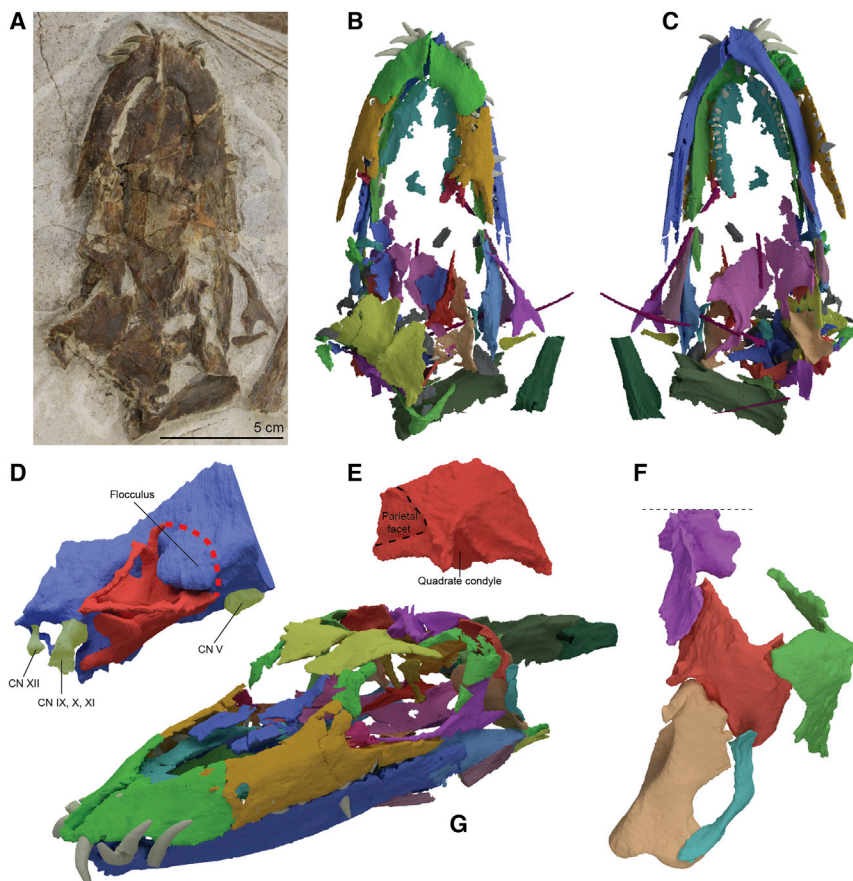


**Figure 1.** The Skull of *Tanystropheus hydroides* sp. nov. Holotype PIMUZ T 2790

(A) The complete skull in dorsal view.  
(B and C) Digital rendering of the skull in dorsal view (B) and ventral view (C). This model is also presented in [Video S1](#).  
(D) Digital rendering of the endocast and endosseous labyrinth (mirrored).  
(E) Digital rendering of the right squamosal in posterolateral view.  
(F) Reconstruction of the temporal region in oblique right lateral view, highlighting the streptostylic articulation of the quadrate and squamosal.  
(G) The digitally “re-assembled” skull of PIMUZ T 2790 in angled left lateral view. This model is also presented in [Video S2](#).

Bone color codings can be found in [Table S1](#). Abbreviations: CN, cranial nerve.

## Horizon

Besano Formation, Anisian-Ladinian boundary, Middle Triassic.

## Diagnosis

The recently revised generic diagnosis for *Tanystropheus* remains valid [17]. The following diagnosis distinguishes *Tanystropheus hydroides* from other *Tanystropheus* species (autapomorphies among Triassic archosauromorphs indicated by an asterisk): premaxilla lacking a postnarial process; single cusped marginal dentition; dentary tooth piercing through a foramen in the maxilla\*; depression on the dorsal surface of the nasals; straight suture between frontals; fused parietal; conspicuously hooked dorsal quadrate head; wide and anteriorly rounded vomers with a single row of large recurved teeth along its outer margin\*; edentulous palatine and pterygoid; dentary bearing a distinct ventral keel at its anterior end\*; a maximum total length of over 5 m.

## Cranial Description of *Tanystropheus hydroides*

The fossilized skull of PIMUZ T 2790 is heavily compressed, obscuring much of its anatomy (Figure 1A). However, the compression caused individual bones to disarticulate rather than deform, so they largely maintain their three-dimensional morphology. Furthermore, the dorsal part of the skull has been displaced posteriorly, essentially folding over the rest of the skull bones. Consequently, many of the bones of the posterior part of the skull are well preserved underneath the large frontals, which

cover them. The digital models rendered from the SRμCT dataset allow the elements to be placed into their *in vivo* position, thus “re-assembling” the skull (Figures 1G and 2). The skull is virtually complete and only parts of the nasal and anterior palatal elements are missing. For some paired bones, only a single element was well preserved, in which case a copied and mirrored version of the best-represented or only available element was added to the digital model in Blender (see [Table S1](#)).

The digital model of PIMUZ T 2790, supplemented by information from other specimens, allows for the detailed reconstruction of the skull of *T. hydroides* (Figures 3A–3C), which strongly deviates from the previous reconstruction of the large morphotype of *T. longobardicus* [4].

The premaxilla is dorsoventrally tall and lacks both prenarial and postnarial processes that are common in early archosauromorphs and of which the latter is well developed in *T. longobardicus* (Figures 2 and 3) [1, 18]. It bears six long, curved fangs, of which the anterior three are the largest and interlocked with the corresponding fangs of the dentary to form a “fish-trap” dentition, similar to that described for Triassic sauroptrygian predators such as *Nothosaurus jagsteus* (SMNS 56618) and *Yunguisaurus liae* (NMNS 004529/F003862) [19, 20]. The maxillary teeth are smaller and peg-like; they are largest at mid-length of the maxilla and gradually reduce in size toward the anterior and posterior ends of the bone. Marginal dentition was subthecodont, with all teeth lacking serrations but bearing clear proximodistal striations. The tenth dentary tooth pierced through the maxilla above. This can be observed on both sides of PIMUZ T 2790, and a similar opening is also present in the right maxilla of *T. hydroides* specimen PIMUZ T 2819 (Figures S1A and S1B). The maxilla curves strongly medially at its dorsal margin, indicating that the nasals were entirely dorsal facing and only minimally visible in lateral view.

Only fragments of the nasals are preserved in PIMUZ T 2790, but they bear a clear concavity, which can also be seen on the

# Current Biology Report

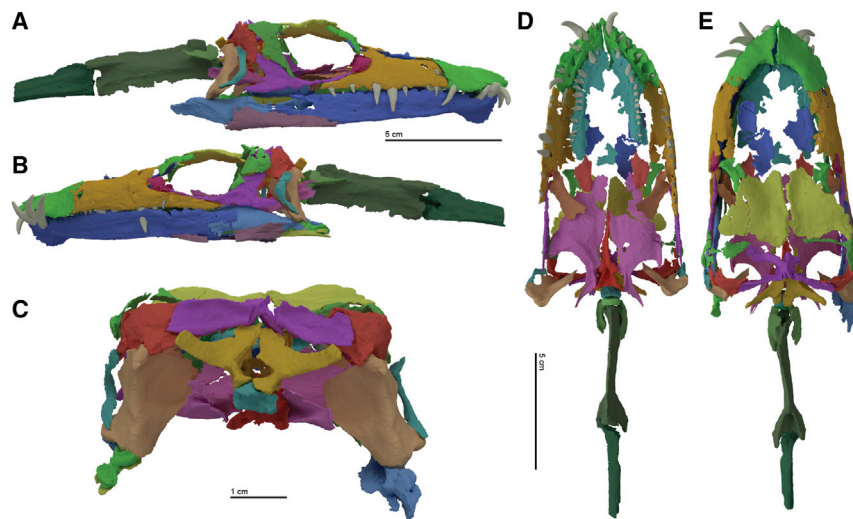


**Figure 2. The Complete “Re-assembled” Digital Model of PIMUZ T 2790**

(A–E) Right lateral (A), left lateral (B), occipital (C), ventral (D), and dorsal view (E). This model is also presented in [Video S2](#). Bone color codings can be found in [Table S1](#).

fragmentary nasal remains of PIMUZ T 2819 ([Figures S1A](#) and [S1B](#), see also figure 3 of [21]). This concavity resembles the narial recess of the closely related, aquatic archosauromorph *Dinocephalosaurus orientalis* (IVPP V13767) [22]. The outline of the nasal and its articulation with the frontal can be inferred from the *T. hydroides* specimen PIMUZ T 2787 ([Figure S2B](#)), which reveals that the nasals were broad, plate-like elements, with an anterolateral process, but lacking an anteromedial process. The absence of the anteromedial process of the nasal and the prenarial process of the premaxilla implies that an internarial bar was absent and that the external nares were confluent. As such, the overall construction of the snout and external nares is reminiscent of that of crown-group crocodylians, in particular that of *Purussaurus* spp. ([Figure 3B](#)) [23].

The frontals are unfused and very broad, largely flattened elements. As such, they formed a wide surface of the skull roof above the orbits, which were largely laterally facing ([Figures 2–3B](#)). The lateral margin of each frontal is slightly curved and forms the dorsal rim of each orbit.

The configuration of the temporal region of *Tanystropheus* differs strongly from that of other early archosauromorphs. The supratemporal fenestrae are entirely dorsally facing, and the intertemporal bar is formed jointly by a dorsoventrally tall postorbital and squamosal ([Figure 1F](#)). The fused parietal possesses pronounced anterolateral and posterolateral processes and bears deep, largely laterally facing supratemporal fossae ([Figure 3B](#)). The squamosal bears a peculiar socket for the reception of the quadrate on its posteroventral surface ([Figure 1E](#)). This socket is profoundly deep and was likely covered by a cartilaginous cap. The dorsal head of the quadrate is extended posteriorly to form a posteroventrally directed hook ([Figure 1F](#)), similar to that described for the allokotosaur *Azendohsaurus madagaskarensis* (FMNH PR 2751) [24]. The posteriorly enlarged articulation surface on the dorsal head of the quadrate and the deep socket on the squamosal allowed for an anteroposteriorly sliding contact between them. This indicates the presence of streptostyly, or the ability of the quadrate to move independently of other cranial bones [25], which has previously been tentatively suggested for *Tanystropheus* [4]. A quadratojugal is identified

confidently for the first time in *Tanystropheus*. It is a small and curved, rod-like bone ([Figures 1F](#), [2](#), and [3](#)). It connects to a facet on the lateroventral condyle of the quadrate ventrally and on its dorsal end to the squamosal and dorsolateral portion of the quadrate. As such, it does not contact the posterior process of the jugal, and thus the infratemporal bar is incomplete.

The palatal elements almost completely

enclosed the palatal surface, similar to *D. orientalis* (IVPP V13898) [22]. The internal choanae were narrow, as indicated by the wide and plate-like vomers. The vomer has a continuously curved outer margin, along which a single row of 15 enlarged recurved teeth is arranged ([Figure S2A](#)). The anterior rami of the pterygoids are poorly preserved in PIMUZ T 2790, but their shape can be inferred from PIMUZ T 2787, which reveals that they were wide and anteriorly rounded ([Figure S2C](#)). Both the pterygoid and palatine are edentulous. This is in stark contrast to *T. longobardicus*, in which the shape of the vomer, palatine, and pterygoid is distinctly different and all these elements are tooth-bearing ([Figure 3F](#)) [17]. The ectopterygoid identified in PIMUZ T 2790 differs strongly in shape from former interpretations, as this element was probably misidentified previously ([Figures 2D](#) and [3C](#)) [4].

The SR $\mu$ CT data also allow for the first detailed observation of the braincase of *Tanystropheus* and reveal the presence of a small laterosphenoid that dorsally encloses the opening for cranial nerve V ([Figure S1C](#)). This represents the most stemward known occurrence of a laterosphenoid in the archosaur lineage [26–28]. The excellent preservation of the braincase also allowed for the partial reconstruction of the endocast and endosseous labyrinth ([Figure 1D](#)). The flocculus, part of the cerebellum, forms a laterally protruding, bulbous lobe in *T. hydroides*. The endosseous labyrinth is complete except for the anterior semicircular canal. However, its shape can be roughly inferred from the shape of the flocculus, over which this canal would have curved.

The dentary bears a distinct ventral keel at its anterior end, which is absent in *T. longobardicus* ([Figures 2A](#), [2B](#), and [3](#)). The posterior margin of the glenoid fossa forms a short vertical bony protrusion that would have prevented the quadrate from dislocating from the mandible during retraction. The articular forms a distinct but not upturned retroarticular process.

## DISCUSSION

### The Lifestyle of *T. hydroides* and *T. longobardicus*

Inferences for the diet of *T. hydroides* can be made based on stomach contents that have been identified in at least two

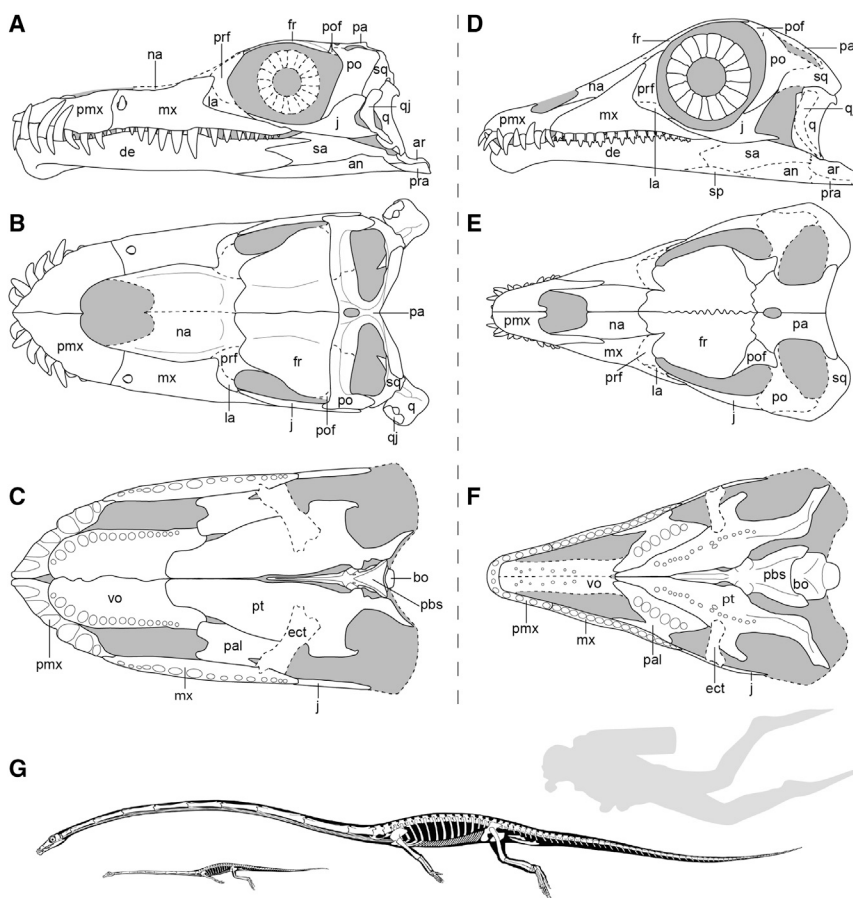


**Figure 3. Interpretative Reconstruction Drawings of *Tanystropheus hydrooides* sp. nov. and *Tanystropheus longobardicus***

(A–F) Reconstruction drawings of the skull and mandible of *Tanystropheus hydrooides* sp. nov. in (A) left lateral, (B) dorsal, and (C) ventral view, and *Tanystropheus longobardicus* in (D) left lateral, (E) dorsal, and (F) ventral view. A revision of the cranial morphology of *Tanystropheus longobardicus* is provided in Methods S1. Important morphological details from *Tanystropheus* specimens other than the SRuCT-scanned PIMUZ T 2790 can be found in Figures S1 and S2, in addition to a digital rendering of the right braincase showing the laterosphenoid in PIMUZ T 2790.

(G) Complete skeletal reconstructions of *Tanystropheus hydrooides* and *Tanystropheus longobardicus* with the outline of a 170-cm-tall human in scuba diving equipment for scale. Abbreviations: an, angular; ar, articular; bo, basisphenoid; de, dentary; ect, ectopterygoid; fr, frontal; j, jugal; la, lacrimal; mx, maxilla; na, nasal; pa, parietal; pal, palatine; pbs, parabasisphenoid; pmx, premaxilla; po, postorbital; pof, postfrontal; pra, prearticular; prf, prefrontal; pt, pterygoid; q, quadrate; qj, quadratojugal; sq, squamosal; vo, vomer.

different specimens. In PIMUZ T 2793, a large number of belemnoid cephalopod hooklets are scattered in the area between the articulated gastralia, and in PIMUZ T 2817, a large accumulation of ganoid fish scales is present in the stomach region [4]. The new skull reconstruction adds crucial information vital to confidently assess the paleobiology and feeding mechanism of *T. hydrooides*. Suction feeding can be excluded since the lower jaws are tightly connected at the symphysis, and they could therefore not move independently from each other to produce the required expansion of the buccal cavity. The hyoid apparatus of *Tanystropheus* also lacks an ossified hyoid corpus or robust hyobranchial elements, which represent important adaptations for suction feeding in amniotes [4, 29, 30]. Furthermore, the large fang-like anterior teeth of *T. hydrooides* would interfere with the prey item entering the buccal cavity during suction feeding. The most likely feeding strategy for *T. hydrooides* is that of a “ram-feeder” (sensu [30]). By employing a laterally directed snapping bite, a prey item would be secured by the procumbent fang-like marginal teeth, aided by the second row of sharp teeth on the outer margin of the vomers. The flattened shape of the snout and the placement of the external nares on its dorsal surface support an at least semi-aquatic lifestyle for *T. hydrooides* and would have reduced drag when the head was moved laterally (Figures 2 and 3A).

The poor hydrodynamic profile and limited appendicular adaptations to an aquatic lifestyle indicate that both *T. hydrooides* and *T. longobardicus* were neither fast nor efficient

swimmers (Figure 3G) [1, 31], unlike the closely related *D. orientalis* [22, 32]. Furthermore, the elongate and gracile semicircular canals of the endosseous labyrinth of *T. hydrooides* reveal that it did not have a pelagic or deep-diving lifestyle

(Figure 1D) [33–36]. This indicates that *T. hydrooides* was likely restricted to coastal and possibly freshwater environments, which is supported by the occurrence of *Tanystropheus*-like cervical vertebrae in fluvial deposits in North America [37]. It is highly unlikely that *T. hydrooides* was able to catch fast-moving prey such as actinopterygian fishes and belemnoid cephalopods through active pursuit. Rather, it seems that *T. hydrooides* was an ambush predator. The head is particularly small given the overall size of the animal and is positioned on an extraordinarily long and slender neck. Therefore, *T. hydrooides* might have been able to approach its prey while being positioned on the seafloor or let its prey approach it without triggering a flight response, especially in turbid water, as has also been hypothesized for certain long-necked plesiosaurs [31, 38].

#### Niche Partitioning in a Highly Specialized Reptile

Lines of arrested growth (LAGs) are periodically formed when bone growth is drastically slowed down during cyclical annual events that reduce metabolism and energy intake (e.g., cold seasons or dry periods) and can therefore be used to approximate the age of an individual [39, 40]. When LAGs occur in close succession at the outer margin of the cortex (i.e., outer circumferential layer, OCL), this implies that growth in the individual had drastically decreased, indicating skeletal maturity. The combined presence of a large number of LAGs and an OCL in the limb elements of the small morphotype specimen PIMUZ T 1277 is a clear indication that this individual was skeletally mature when it

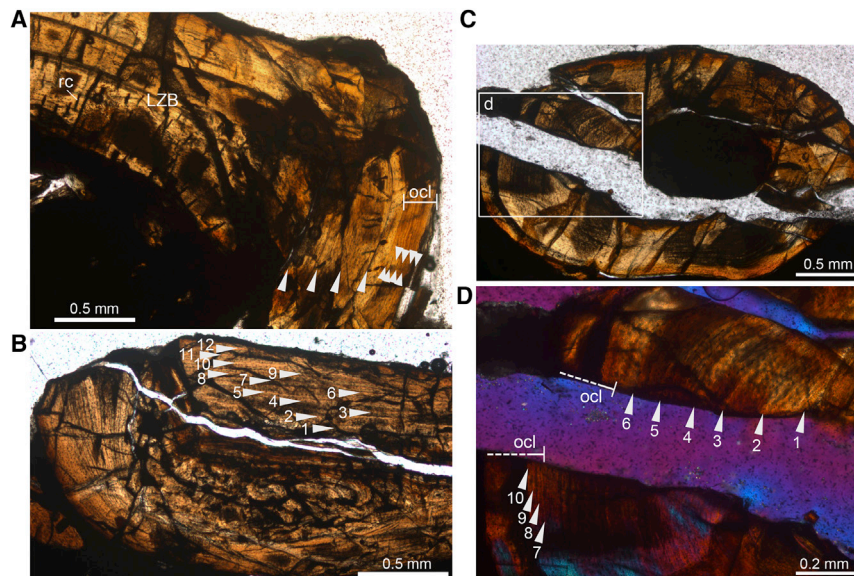


**Figure 4. Paleohistological Sections of *Tanystropheus longobardicus***

(A) Close-up of the cortex of the femur of PIMUZ T 1277 in normal transmitted light.

(B) Close-up of the cortex of the femur of PIMUZ T 2484 in normal transmitted light.

(C and D) Overview of complete cross-section and close-up of the cortex of the zeugopodial element of PIMUZ T 1277. Image (C) in normal transmitted light; image (D) in cross-polarized light using lambda compensator.

Small arrow heads in (A) indicate growth marks within the cortical outer circumferential layer, whereas larger arrow heads generally indicate LAGs in the deeper parts of the cortex. Abbreviations: Lzb, lamellar-zonal bone; ocl, outer circumferential layer (= external fundamental system); rc, radial vascular canals. All histological samples are presented in Figure S3 and described in Methods S1.

died (Figures 4A, C, and D) [41]. The total body length of PIMUZ T 1277 is approximately 1.5 m [5], whereas the largest known specimen of *T. hydrooides* is more than 3.5 times longer (Figure 3G) [4]. From this large size discrepancy, it can be unequivocally determined that the specimens bearing tricuspid teeth represent a small species distinct from *T. hydrooides*. Together with their distinctly different dentitions (Figures 3A–3F), this implies that *T. hydrooides* and *T. longobardicus* certainly exploited different food sources. The tricuspid dentition seen in *T. longobardicus* has a broad utilization among extant squamates and is widespread among insectivores and omnivores [42]. Therefore, a possible broad diet composed of small animals including soft-shelled invertebrates such as decapod crustaceans is here proposed for this species.

Both *T. hydrooides* and *T. longobardicus* are known from several articulated and disarticulated specimens from the Besano Formation of Monte San Giorgio. Although it cannot be excluded that the carcasses of these taxa were transported to their bedding position after death, both species show a similar taphonomic pattern [9], and it is most likely that both taxa co-occurred in the same habitat. The clear distinction in feeding strategy thus presents a strong indication of niche partitioning between these two species. Niche partitioning has previously been reported for Mesozoic marine reptiles [43, 44] and was tentatively suggested for *Tanystropheus* material from the Middle Triassic Makhtesh Ramon locality of Israel [17, 45]. Niche partitioning has also been invoked for the actinopterygian *Saurichthys* [8, 46, 47] and among perleidid fishes [48] from the Middle Triassic of Monte San Giorgio. Indeed, habitat partitioning appears to be a repeated pattern in Triassic marine basin biota. It is remarkable that such a striking partitioning occurred comparatively soon after the End-Permian mass extinction in a highly specialized genus. Previously, it was considered that the neck of *Tanystropheus* formed a morphological constraint and severely limited its ecological adaptability [49, 50]. Our findings reveal that the neck of *Tanystropheus* was more multifunctional than previously considered and allowed for the exploitation of

various food sources. Furthermore, the wide distribution of specimens that are morphologically indistinguishable from *T. hydrooides* across the Tethys basin highlights the efficiency of the *Tanystropheus* bauplan [6, 17].

## Conclusions

Reconstructing the morphology and paleobiology of long extinct organisms without close modern analogs is crucial in our understanding of biological diversity through time and approximating the ecomorphological limitations of life. The bizarre *Tanystropheus* represents a particularly interesting case study in this regard due to its unique morphology among tetrapods, exemplified by its extremely long neck consisting of only 13 very elongate vertebrae. The skull reconstruction based on PIMUZ T 2790 deviates strongly from that of other early archosauromorphs and reveals that *T. hydrooides* hunted in an aquatic environment, using its long fang-like teeth and a lateral snapping bite to seize its prey. *Tanystropheus hydrooides* and *T. longobardicus* were two closely related species that almost certainly co-occurred in the same habitat. This remarkable case of niche partitioning highlights the versatility of the *Tanystropheus* bauplan and the complexity of Middle Triassic marine trophic networks within 10 million years after the End-Permian extinction event, and the major role of reptiles therein.

## STAR★METHODS

Detailed methods are provided in the online version of this paper and include the following:

- **KEY RESOURCES TABLE**
- **RESOURCE AVAILABILITY**
  - Lead contact
  - Materials availability
  - Data and code availability
  - Institutional repositories
- **EXPERIMENTAL MODEL AND SUBJECT DETAILS**

● METHOD DETAILS

- Synchrotron micro Computer Tomography acquisition and image processing
- Bone histology

● QUANTIFICATION AND STATISTICAL ANALYSIS

- Phylogenetic analysis

SUPPLEMENTAL INFORMATION

Supplemental Information can be found online at <https://doi.org/10.1016/j.cub.2020.07.025>.

ACKNOWLEDGMENTS

We are very thankful for the full-body skeletal reconstructions of the two *Tanystropeus* species by Beat Scheffold (PIMUZ). Christian Klug (PIMUZ) is thanked for specimen access and allowing us to remove the skull of PIMUZ T 2790 from the larger slab. Dylan Bastiaans, Feiko Miedema, Christian Klug, Roger Benson, Erin Saupe, Jonah Choiniere, Roland Sookias, Richard Butler, Fabio Dalla Vecchia, Pernille Troelsen, Oliver Rauhut, Gabriela Sobral, and Dennis Voeten are thanked for fruitful discussions. We thank the European Synchrotron Radiation Facility (ESRF), Grenoble, France, for provision of synchrotron radiation beamtime at beamline BM05. This study is part of the SNSF Project granted to T.M.S. (grant no. 2'5321-162775). J.M.N. was funded by a Leverhulme Trust Early Career Fellowship (ECF-2017-360). We kindly thank editor Florian Maderspacher and two anonymous reviewers for their helpful suggestions, which improved the quality of this manuscript.

AUTHOR CONTRIBUTIONS

S.N.F.S., T.M.S., N.C.F., O.R., and S.N. designed the study. V.F. and S.N.F.S. performed the synchrotron scanning and processed the data. S.N.F.S. segmented the skull. J.M.N. and S.N.F.S. segmented the endocast and endosseous labyrinth. T.M.S. and S.N.F.S. made the histological sections. S.N.F.S. performed the phylogenetic analysis. S.N.F.S. and T.M.S. made the figures. S.N.F.S., T.M.S., and V.F. wrote the manuscript. All authors reviewed a final draft of the manuscript.

DECLARATION OF INTERESTS

The authors declare no competing interests.

Received: June 7, 2020

Revised: June 30, 2020

Accepted: July 8, 2020

Published: August 6, 2020

REFERENCES

1. Nosotti, S. (2007). *Tanystropeus longobardicus* (Reptilia, Protorosauria): Re-interpretations of the anatomy based on new specimens from the Middle Triassic of Besano (Lombardy, northern Italy). *Memorie della Società Italiana di Scienze Naturali e del Museo Civico di Storia Naturale di Milano* 35, 1–88.
2. Peyer, B. (1931). Die Triasfauna der Tessiner Kalkalpen II. *Tanystropeus longobardicus* Bass. sp. *Abhandlungen der Schweizerischen Paläontologischen Gesellschaft* 50, 1–110.
3. Tschanz, K. (1986). Funktionelle Anatomie der Halswirbelsäule von *Tanystropeus longobardicus* (Bassani) aus der Trias (Anis/Ladin) des Monte San Giorgio (Tessin) auf der Basis vergleichend morphologischer Untersuchungen an der Halsmuskulatur rezenten Echsen. PhD thesis (Universität Zürich).
4. Wild, R. (1973). Die Triasfauna der Tessiner Kalkalpen XXII. *Tanystropeus longobardicus* (Bassani) (Neue Ergebnisse). *Schweizerische Paläontologische Abhandlungen* 95, 1–162.
5. Wild, R. (1980). Neue Funde von *Tanystropeus* (Reptilia, Squamata). *Schweizerische Paläontologische Abhandlungen* 102.
6. Rieppel, O., Jiang, D.-Y., Fraser, N.C., Hao, W.-C., Motani, R., Sun, Y.-L., and Sun, Z.-Y. (2010). *Tanystropeus cf. T. longobardicus* from the early Late Triassic of Guizhou Province, southwestern China. *J. Vertebr. Paleontol.* 30, 1082–1089.
7. Taylor, M.P., and Wedel, M.J. (2013). Why sauropods had long necks; and why giraffes have short necks. *PeerJ* 1, e36.
8. Stockar, R. (2010). Facies, depositional environment, and palaeoecology of the Middle Triassic Cassina beds (Meride Limestone, Monte San Giorgio, Switzerland). *Swiss J. Geosci.* 103, 101–119.
9. Beardmore, S.R., and Furrer, H. (2017). Land or water: using taphonomic models to determine the lifestyle of the Triassic protorosaur *Tanystropeus* (Diapsida, Archosauromorph). *Palaeobiodiversity and Palaeoenvironments* 98, 243–258.
10. Jaquier, V.P., and Scheyer, T.M. (2017). Bone Histology of the Middle Triassic Long-Necked Reptiles *Tanystropeus* and *Macrocnemus* (Archosauromorph, Protorosauria). *J. Vertebr. Paleontol.* 37.
11. Renesto, S. (2005). A new specimen of *Tanystropeus* (Reptilia Protorosauria) from the Middle Triassic of Switzerland and the ecology of the genus. *Rivista Italiana di Paleontologia e Stratigrafia* 111, 377–394.
12. Renesto, S., and Saller, F. (2018). Evidences for a semi aquatic life style in the Triassic diapsid reptile *Tanystropeus*. *Rivista Italiana di Paleontologia e Stratigrafia* 124, 23–34.
13. Osborn, H.F. (1903). The reptilian subclasses Diapsida and Synapsida and the early history of the Diapsidia. *Memoirs of the American Museum of Natural History* 1, 449–519.
14. Huene, F.R.V. (1946). Die grossen Stämme der Tetrapoden in den geologischen Zeiten. *Biol. Zent. Bl.* 65, 268–275.
15. Camp, C.L. (1945). *Prolacerta* and the protorosaurian reptiles. Part I and Part II. *Am. J. Sci.* 243, 17–32, 84–101.
16. Meyer, H.v. (1855). Die Saurier des Muschelkalkes mit Rücksicht auf die Saurier aus buntem Sandstein und Keuper. In *Zur Fauna der Vorwelt, zweite Abtheilung*, H. Keller, m. Frankfurt, ed. (Heinrich Keller).
17. Spiekman, S.N.F., and Scheyer, T.M. (2019). A taxonomic revision of the genus *Tanystropeus* (Archosauromorph, Tanystropeidae). *Palaeontologia Electronica* 22, 1–46.
18. Ezcurra, M.D. (2016). The phylogenetic relationships of basal archosauromorphs, with an emphasis on the systematics of proterosuchian archosauriforms. *PeerJ* 4, e1778.
19. Rieppel, O. (2002). Feeding mechanics in Triassic stem-group sauropterygians: the anatomy of a successful invasion of Mesozoic seas. *Zool. J. Linn. Soc.* 135, 33–63.
20. Cheng, Y.-N., Sato, T., Wu, X.-C., and Li, C. (2006). First complete pistosauroid from the Triassic of China. *J. Vertebr. Paleontol.* 26, 501–504.
21. Jiang, D.-Y., Rieppel, O., Fraser, N.C., Motani, R., Hao, W.-C., Tintori, A., et al. (2011). New information on the protorosaurian reptile *Macrocnemus fuyuanensis* Li et al., 2007, from the Middle/Upper Triassic of Yunnan, China. *Journal of Vertebrate Paleontology* 31, 1230–1237.
22. Rieppel, O., Li, C., and Fraser, N.C. (2008). The skeletal anatomy of the Triassic protorosaur *Dinocephalosaurus orientalis*, from the Middle Triassic of Guizhou Province, southern China. *J. Vertebr. Paleontol.* 28, 95–110.
23. Aguilera, O.A., Riff, D., and Bocquentin-Villanueva, J. (2006). A new giant *Purussaurus* (Crocodyliformes, Alligatoridae) from the upper Miocene Urumaco formation, Venezuela. *Journal of Systematic Palaeontology* 4, 221–232.
24. Flynn, J.J., Nesbitt, S.J., Michael Parrish, J., Ranivoharimana, L., and Wyss, A.R. (2010). A new species of *Azendohsaurus* (Diapsida: Archosauromorph) from the Triassic Isalo Group of southwestern Madagascar: cranium and mandible. *Palaeontology* 53, 669–688.
25. Smith, K.K. (1980). Mechanical significance of streptostyly in lizards. *Nature* 283, 778–779.

# Current Biology Report



26. Clark, J.M., Welman, J., Gauthier, J.A., and Parrish, J.M. (1993). The laterosphenoid bone of early archosauriforms. *J. Vertebr. Paleontol.* 13, 48–57.
27. Sobral, G., and Müller, J. (2019). The braincase of *Mesosuchus browni* (Reptilia, Archosauromorpha) with information on the inner ear and description of a pneumatic sinus. *PeerJ* 7, e6798.
28. Sobral, G., Sookias, R.B., Bhullar, B.-A.S., Smith, R., Butler, R.J., and Müller, J. (2016). New information on the braincase and inner ear of *Euparkeria capensis* Broom: implications for diapsid and archosaur evolution. *R. Soc. Open Sci.* 3, 160072.
29. Lauder, G. (1985). Aquatic feeding in lower vertebrates. In *Functional vertebrate morphology*, M. Hildebrand, D. Bramble, K. Liem, and D. Wake, eds. (Cambridge: Harvard University Press), pp. 210–229.
30. Motani, R., Ji, C., Tomita, T., Kelley, N., Maxwell, E., Jiang, D.Y., and Sander, P.M. (2013). Absence of suction feeding ichthyosaurs and its implications for triassic mesopelagic paleoecology. *PLoS ONE* 8, e66075.
31. Massare, J.A. (1988). Swimming capabilities of Mesozoic marine reptiles: implications for method of predation. *Paleobiology* 14, 187–205.
32. Liu, J., Organ, C.L., Benton, M.J., Brindley, M.C., and Aitchison, J.C. (2017). Live birth in an archosauromorph reptile. *Nat. Commun.* 8, 14445.
33. Evers, S.W., Neenan, J.M., Ferreira, G.S., Werneburg, I., Barrett, P.M., and Benson, R.B. (2019). Neurovascular anatomy of the protostegid turtle *Rhinochelys pulchriceps* and comparisons of membranous and endosseous labyrinth shape in an extant turtle. *Zool. J. Linn. Soc.* 187, 800–828.
34. Neenan, J.M., Reich, T., Evers, S.W., Druckenmiller, P.S., Voeten, D.F., Choiniere, J.N., Barrett, P.M., Pierce, S.E., and Benson, R.B. (2017). Evolution of the sauropterygian labyrinth with increasingly pelagic life-styles. *Current Biology* 27, 3852–3858.e3.
35. Neenan, J.M., and Scheyer, T.M. (2012). The braincase and inner ear of *Placodus gigas* (Sauropterygia, Placodontia)—a new reconstruction based on micro-computed tomographic data. *J. Vertebr. Paleontol.* 32, 1350–1357.
36. Schwab, J.A., Young, M.T., Neenan, J.M., Walsh, S.A., Witmer, L.M., Herrera, Y., Allain, R., Brochu, C.A., Choiniere, J.N., Clark, J.M., et al. (2020). Inner ear sensory system changes as extinct crocodylomorphs transitioned from land to water. *Proc. Natl. Acad. Sci. USA* 117, 10422–10428.
37. Formoso, K.K., Nesbitt, S.J., Pritchard, A.C., Stocker, M.R., and Parker, W.G. (2019). A long-necked tanystropheid from the Middle Triassic Moenkopi Formation (Anisian) provides insights into the ecology and biogeography of tanystropheids. *Palaeontologia Electronica* 22, 1–15.
38. Wintrich, T., Jonas, R., Wilke, H.-J., Schmitz, L., and Sander, P.M. (2019). Neck mobility in the Jurassic plesiosaur *Cryptoclidus eurymerus*: finite element analysis as a new approach to understanding the cervical skeleton in fossil vertebrates. *PeerJ* 7, e7658.
39. Chinsamy, A. (1993). Bone histology and growth trajectory of the prosauropod dinosaur *Massospondylus carinatus* Owen. *Modern Geology* 18, 319–329.
40. Köhler, M., Marín-Moratalla, N., Jordana, X., and Aanes, R. (2012). Seasonal bone growth and physiology in endotherms shed light on dinosaur physiology. *Nature* 487, 358–361.
41. Woodward, H.N., Horner, J.R., and Farlow, J.O. (2011). Osteohistological evidence for determinate growth in the American alligator. *J. Herpetol.* 45, 339–343.
42. Melstrom, K.M. (2017). The relationship between diet and tooth complexity in living dentigerous saurians. *J. Morphol.* 278, 500–522.
43. Rieppel, O., Mazin, J.-M., and Tchernov, E. (1997). Speciation along rifting continental margins: a new nothosaur from the Negev (Israel). *Comptes Rendus de l'Académie des Sciences* 325, 991–997.
44. Foffa, D., Young, M.T., Stubbs, T.L., Dexter, K.G., and Brusatte, S.L. (2018). The long-term ecology and evolution of marine reptiles in a Jurassic seaway. *Nat. Ecol. Evol.* 2, 1548–1555.
45. Rieppel, O. (2001). A new species of *Tanystropheus* (Reptilia: Protorosauria) from the Middle Triassic of Makhtesh Ramon, Israel. *Neues Jahrb. Geol. Paläontol. Abh.* 221, 271–287.
46. Rieppel, O. (1985). Die Triasfauna der Tessiner Kalkalpen: XXV. Die Gattung *Saurichthys* (Pisces, Actinopterygii) aus der mittleren Trias des Monte San Giorgio, Kanton Tessin. *Schweizerische Paläontologische Abhandlungen* 108, 1–81.
47. Rieppel, O. (1992). A new species of the genus *Saurichthys* (Pisces: Actinopterygii) from the Middle Triassic of Monte San Giorgio (Switzerland), with comments on the phylogenetic interrelationships of the genus. *Palaeontographica Abt. A Paläozoologie - Stratigraphie* 221, 63–94.
48. Bürgin, T. (1996). Diversity in the feeding apparatus of perleidid fishes (Actinopterygii) from the Middle Triassic of Monte San Giorgio (Switzerland). In *Mesozoic Fishes – Systematics and Paleoecology*, G. Arratia, and G. Viohl, eds. (Munich: F. Pfeil).
49. Wild, R. (1987). An example of biological reasons for extinction: *Tanystropheus* (Reptilia, Squamata) (Mémoires de la Société Géologique de France).
50. Taylor, M.A. (1989). Neck and neck. *Nature* 341, 668–689.
51. Goloboff, P.A., and Catalano, S.A. (2016). TNT version 1.5, including a full implementation of phylogenetic morphometrics. *Cladistics* 32, 221–238.
52. Cau, A., Beyrand, V., Voeten, D.F.A.E., Fernandez, V., Tafforeau, P., Stein, K., Barsbold, R., Tsogtbaatar, K., Currie, P.J., and Godefroit, P. (2017). Synchrotron scanning reveals amphibious ecomorphology in a new clade of bird-like dinosaurs. *Nature* 552, 395–399.
53. Mirone, A., Brun, E., Gouillart, E., Tafforeau, P., and Kieffer, J. (2014). The PyHST2 hybrid distributed code for high speed tomographic reconstruction with iterative reconstruction and a priori knowledge capabilities. *Nucl. Instrum. Methods Phys. Res. B* 324, 41–48.
54. Paganin, D., Mayo, S.C., Gureyev, T.E., Miller, P.R., and Wilkins, S.W. (2002). Simultaneous phase and amplitude extraction from a single defocused image of a homogeneous object. *J. Microsc.* 206, 33–40.
55. Lykkegaard, A., Johnson, G., and Tafforeau, P. (2011). Correction of ring artifacts in X-ray tomographic images. *International Journal of Tomography & Statistics* 18, 1–9.
56. Chinsamy, A., and Raath, M.A. (1992). Preparation of fossil bone for histological examination. *Palaeontologia Africana* 29, 39–44.
57. Pritchard, A.C., Turner, A.H., Nesbitt, S.J., Irmis, R.B., and Smith, N.D. (2015). Late Triassic tanystropheids (Reptilia, Archosauromorpha) from Northern New Mexico (Petrified Forest Member, Chinle Formation) and the biogeography, functional morphology, and evolution of Tanystropheidae. *J. Vertebr. Paleontol.* 35, e911186.
58. Nesbitt, S.J., Flynn, J.J., Pritchard, A.C., Parrish, J.M., Ranivoharimana, L., and Wyss, A.R. (2015). Postcranial anatomy and relationships of *Azendohsaurus madagaskarensis*. *Bulletin of the American Museum of Natural History* 398, 1–126.
59. Pritchard, A.C., and Nesbitt, S.J. (2017). A bird-like skull in a Triassic diapsid reptile increases heterogeneity of the morphological and phylogenetic radiation of Diapsida. *R. Soc. Open Sci.* 4, 170499.
60. Pritchard, A.C., Turner, A.H., Irmis, R.B., Nesbitt, S.J., and Smith, N.D. (2016). Extreme Modification of the Tetrapod Forelimb in a Triassic Diapsid Reptile. *Curr. Biol.* 26, 2779–2786.
61. Pritchard, A.C., Gauthier, J.A., Hanson, M., Bever, G.S., and Bhullar, B.S. (2018). A tiny Triassic saurian from Connecticut and the early evolution of the diapsid feeding apparatus. *Nat. Commun.* 9, 1213.
62. Scheyer, T.M., Spiekman, S.N.F., Sues, H.D., Ezcurra, M.D., Butler, R.J., and Jones, M.E.H. (2020). *Colobops*: a juvenile rhynchocephalian reptile (Lepidosauromorpha), not a diminutive archosauromorph with an unusually strong bite. *R. Soc. Open Sci.* 7, 192179.
63. Benton, M.J., and Allen, J.L. (1997). *Boreopricea* from the Lower Triassic of Russia, and the relationships of the prolacertiform reptiles. *Palaeontology* 40, 931–953.

## STAR★METHODS

### KEY RESOURCES TABLE

REAGENT or RESOURCE	SOURCE	IDENTIFIER
<b>Biological Samples</b>		
<i>Tanystropheus hydrooides</i> (skull, mandibles, atlas-axis complex, and cervical vertebra 3)	This paper	PIMUZ T 2790
<i>Tanystropheus longobardicus</i> (femur thin-section)	This paper	PIMUZ T 1277
<i>Tanystropheus longobardicus</i> (zeugopodial element thin-section)	This paper	PIMUZ T 1277
<i>Tanystropheus longobardicus</i> (femur thin-section)	This paper	PIMUZ T 2484
<i>Tanystropheus longobardicus</i> (disarticulated skull)	This paper	PIMUZ T 2484
<i>Tanystropheus hydrooides</i> (skull)	This paper	PIMUZ T 2819
<i>Tanystropheus hydrooides</i> (disarticulated skull)	This paper	PIMUZ T 2787
<b>Deposited Data</b>		
SR $\mu$ CT data of PIMUZ T 2790	This paper	<a href="http://paleo.esrf.fr">http://paleo.esrf.fr</a>
The digital models of PIMUZ T 2790	This paper	<a href="http://paleo.esrf.fr">http://paleo.esrf.fr</a>
Paleohistological thin sections	This paper	Figure S3
Nexus file for phylogenetic analysis	This paper	Document S1
Video files of digital models of PIMUZ T 2790	This paper	Document S1
<b>Software and Algorithms</b>		
Mimics Research v19.0	<a href="https://www.materialise.com/en/medical/mimics-innovation-suite/mimics">https://www.materialise.com/en/medical/mimics-innovation-suite/mimics</a>	N/A
Blender 2.7	<a href="https://blender.org">https://blender.org</a>	N/A
TNT 1.5	[51]	N/A

### RESOURCE AVAILABILITY

#### Lead contact

Further information and requests for resources and reagents should be directed to and will be fulfilled by the Lead Contact, Stephan N.F. Spiekman ([stephanspiekman@gmail.com](mailto:stephanspiekman@gmail.com)).

#### Materials availability

This study did not generate new unique reagents.

#### Data and code availability

The digital models and SR $\mu$ CT data of PIMUZ T 2790 have been deposited at <http://paleo.esrf.fr>. All histological slides used in the study are provided in Figure S3.

#### Institutional repositories

Bayerische Staatssammlung für Paläontologie und Geologie, Munich, Germany (BSPG); Field Museum of Natural History, Chicago, USA (FMNH); Institute of Vertebrate Paleontology and Paleoanthropology, Beijing, China (IVPP); Museo di Storia Naturale, Milan, Italy (MSNM); National Museum of Natural Science, Taichung City, Taiwan (NMNS); Paläontologisches Institut und Museum der Universität Zürich, Zurich, Switzerland (PIMUZ); Staatliches Museum für Naturkunde, Stuttgart, Germany (SMNS).

### EXPERIMENTAL MODEL AND SUBJECT DETAILS

The experimental subjects of this study comprise several fossil specimens belonging to the tanystropheid archosauromorph genus *Tanystropheus*, most notably PIMUZ T 2790, which was subjected to SR $\mu$ CT scanning. *Tanystropheus longobardicus* specimens PIMUZ T 2484 and PIMUZ T 1277 were sectioned for bone histology. The cranial reconstructions of both *Tanystropheus* species were made based on morphological observations of PIMUZ T 2790, PIMUZ T 2819, PIMUZ T 2787, and PIMUZ T 2484. All specimens and histological slides are reposited at the Paleontological Institute and Museum of the University of Zurich, Switzerland (PIMUZ).

## METHOD DETAILS

### Synchrotron micro Computer Tomography acquisition and image processing

The specimen was scanned at the BM05 beamline of the European Synchrotron Radiation Facility (ESRF, Grenoble, France) using propagation phase contrast synchrotron radiation micro-computed tomography. The experimental setup consisted of: filtered white beam (bending magnet, filters: 18 rods of Al, 5 mm in diameter and 10 cm in length, Mo 0.25 mm) with a total integrated detected energy of 115 keV, a sample-detector propagation distance of 4 m and an indirect detector (2 mm LuAG scintillator 0.25x magnification, CCD FReLoN 2K camera) producing data with a measured isotropic voxel size of 46.76  $\mu\text{m}$ . To image the full sample, the center of rotation was shifted to increase the lateral field of view by ~30%, and 77 acquisitions were necessary on the vertical axis (keeping a 50% overlap between consecutive scans). Each acquisition consisted of 2999 projections of a total integration time of 0.3 s (10 frames of 0.03 s per projection in accumulation mode [52]) over a rotation of 360°. Tomographic reconstruction was achieved with PyHST2 [53], using the single distance phase retrieval approach [54]. Post processing included: modification of the bit depth from 32 bits to 16 bits as a stack of tiff, merging of the 77 datasets using a weighted average on overlapping parts, ring correction [55]; cropping of the volume.

The data was segmented and reconstructed in Mimics Research v19.0 (<https://www.materialise.com/en/medical/mimics-innovation-suite/mimics>; Materialise NV, Leuven, Belgium). The models of the individual elements were imported as PLY files into Blender 2.7 (<https://blender.org>; Stitching Blender Foundation, Amsterdam, the Netherlands), a 3D modeling and visualization program in which the elements could be rotated and moved independently, and images could be rendered, applying colors and texture to the models. As an aid to establish bone contacts, most elements were printed using a MakerBot Replicator 2X 3D printer (<https://makerbot.com>; MakerBot Industries, LLC, New York City, USA). This way, using both the digital and printed models, the connections between the bones could be restored in high detail, allowing for the confident reconstruction of the skull.

### Bone histology

Three bones of two separate specimens of *T. longobardicus* were sampled for analysis of bone histology. From PIMUZ T 1277 we sampled a femur and a zeugopodial element and from PIMUZ T 2484, we sampled a femur. Thin slices of the bones were removed from the slabs using a small diamond-studded saw blade on a Dremel drill. The samples were then embedded in synthetic resin and ground down to about 60–100 microns thick slides using SIC powders (220, 500 and 800), following standard protocols [56]. The thin-sections were studied and photographed using a LEICA compound microscope DM 2500 M equipped with digital camera DFC 420C (an overview of the slides can be found in Figure S3).

## QUANTIFICATION AND STATISTICAL ANALYSIS

### Phylogenetic analysis

The interrelationships of tanystropheid archosauromorphs have previously been tested with a dedicated character matrix [57], which has subsequently been modified and expanded upon in order to investigate broader archosauromorph and early diapsid phylogeny [58–60]. We modified the most recent iteration of this matrix [61] in order to evaluate the implications of our findings for tanystropheid and early archosauromorph phylogeny. *Colobops noviportensis* is known from a single skull of a likely very early juvenile individual. Although recovered as an early diverging rhynchosaur in [61], a recent re-analysis of this taxon has revealed it is actually a rhynchocephalian lepidosauromorph [62]. The inclusion of a poorly known rhynchocephalian based on an ontogenetically early specimen is not beneficial in resolving early archosauromorph phylogeny and might introduce unnecessary biases, and therefore *C. noviportensis* was excluded here. *Boreopricea funerea* is also known from a single specimen that is poorly preserved and several elements of this specimen have likely been misplaced, which introduces the possibility of unreliable character observation [18, 63], and it was therefore also excluded. The modifications made to the characters and the updated data matrix can be found in Methods S1. We analyzed the matrix according to the maximum parsimony criterion in TNT 1.5 [51], using the Traditional Search algorithm. The same parameters described in [61] were used to analyze the data and calculate the support values, in order to directly compare results. Three most parsimonious trees with 1125 steps were recovered (CI = 0.324; RI = 0.648) (the complete strict consensus tree, including Bootstrap and Bremer support values, can be found in Figure S4).